catalysts

MDPI

Supplementary Materials

Promotional Effect of Pd Addition on the Catalytic Activity of Composite Pt-Pd/AlSBA-15–β Catalyst for Enhanced *n*-Heptane Hydroisomerization

Karolina Jaroszewska [1,*], Monika Fedyna [2], Aleksandra Masalska [1], Rafał Łużny [1] and Janusz Trawczyński [1]

[1] Department of Fuels Chemistry and Technology, Wrocław University of Science and Technology, 7/9 Gdańska St., PL-50344 Wrocław, Poland; aleksandra.masalska@pwr.edu.pl (A.M.); rafal.luzny@pwr.edu.pl (R.Ł.); janusz.trawczynski@pwr.edu.pl (J.T.)

[2] Faculty of Chemistry, Jagiellonian University in Kraków, 2 Gronostajowa St., PL-30387 Kraków, Poland; monika.fedyna@uj.edu.pl

Correspondence: karolina.jaroszewska@pwr.edu.pl; Tel.: +48-71-320-63-02

Table of Contents

1. RESULTS AND DISCUSSION

1.1. Catalysts characterisation

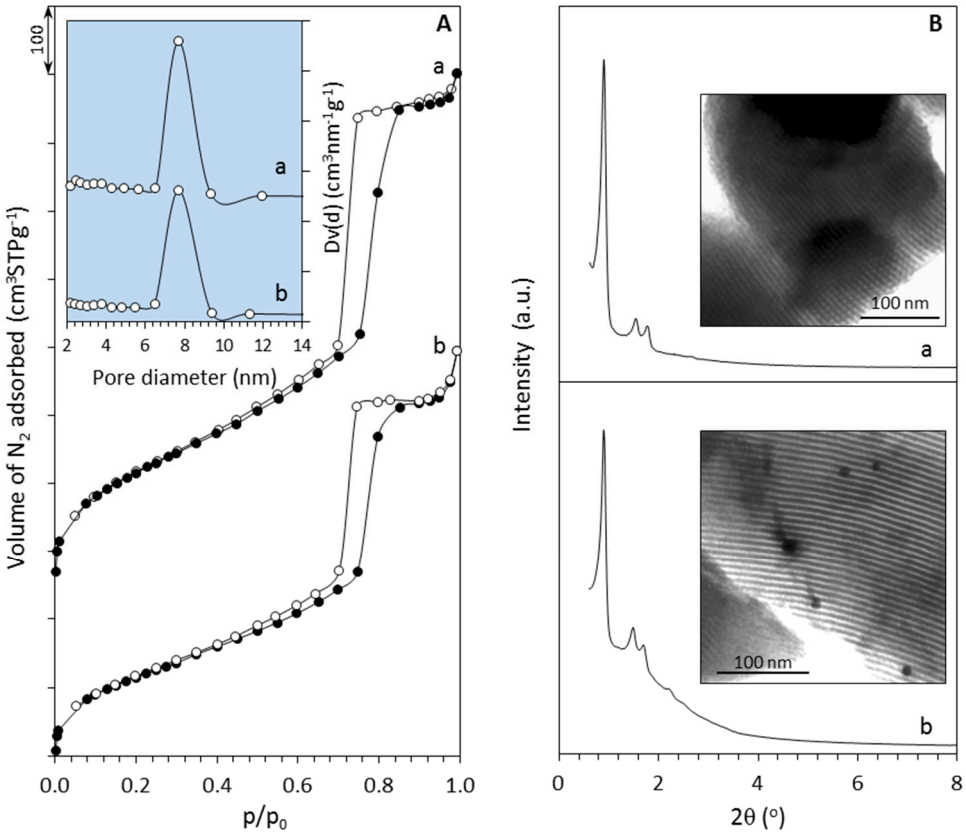

Figure S1. Characterization of the Pt catalysts; **(A)** N_2 adsorption (full symbols) - desorption isotherms (open symbols) and pore size distribution and **(B)** XRD patterns and TEM images of: **(a)** AlSBA-15 and **(b)** Pt/AlSBA-15 samples.

The textural properties of AlSBA-15 and of the reference Pt/AlSBA-15 catalyst were characterised by the low temperature N_2 adsorption–desorption, XRD and TEM techniques. As can be seen, AlSBA-15 material exhibits a type IV of isotherm with the H1 hysteresis loop corresponding to a honeycomb-like mesoporous structure with well-defined cylindrical pore channels (**Figure S1Aa**). The shaping of AlSBA-15 with binder followed by impregnation procedure only slightly changes the textural properties of the Pt/AlSBA-15 catalyst, however it can be observed that the typical shape of isotherms for AlSBA-15 retains (**Figure S1Ab**). Further evidence for a highly ordered hexagonal structure in

AlSBA-15 and Pt/AlSBA-15 is provided by low-angle XRD patterns and TEM micrographs (**Figure S1B**).

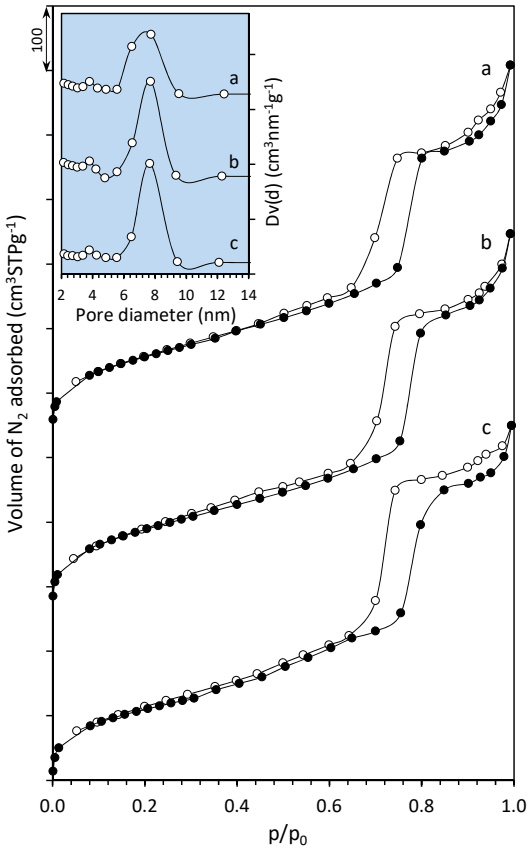

Figure S2. N_2 adsorption–desorption isotherms and pore size distribution (as an inclusion) for: (**a**) Pt/SBA–BEA, (**b**) Pd/SBA–BEA and (**c**) Pt-Pd/SBA–BEA catalysts.

Table S1. Textural properties of the supports and the catalysts.

Sample	S_{BET} (m^2g^{-1})	V_T[a] (cm^3g^{-1})	S_{MES}[b] (m^2g^{-1})	V_{MES}[c] (cm^3g^{-1})	d_{BJH}[d] (nm)
AlSBA-15	788	1.20	634	1.09	7.7
Pt/AlSBA-15	579	0.99	442	0.75	7.9
Pt/BEA	–	0.93	153	–	1.4
Pt/SBA–BEA	524	0.93	302	0.51	7.7
Pt/SBA–MFI	455	0.80	380	0.61	6.5
Pt/SBA–MOR	452	0.80	353	0.58	6.5
Pd/SBA–BEA	581	0.97	420	0.54	7.7
Pt-Pd/SBA–BEA	546	0.92	365	0.49	7.8

[a] Total pore volume determined at p/p_0>0.99; [b,c] Surface and volume of mesopores from t-plot; [d] Pore diameter (BJH method).

For the composite catalysts (the Pt-, Pd- and Pt-Pd/SBA–BEA catalysts are presented as the examples on **Figure S2**), the shape of the isotherms is similar to the Pt/AlSBA-15 one (**Figure S1**). As can be expected, all composite catalysts show lower S_{BET} in comparison to the Pt/AlSBA-15 sample, what is a consequence of the preparation procedure involving not only the shaping with a binder and metallic phase deposition but also the zeolite adding into AlSBA-15 (**Table S1**). However, a clear indication for a presence of an ordered

hexagonal structure in the investigated catalysts is also provided by the low-angle XRD diffractograms (**Figure S3**).

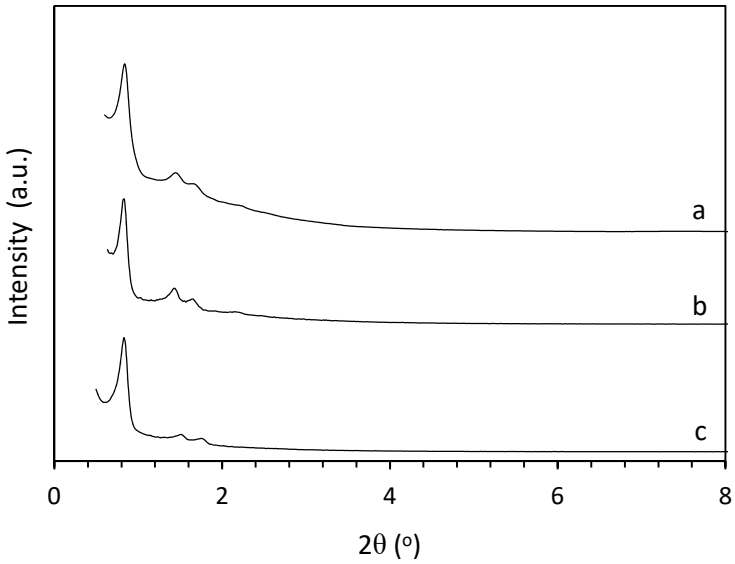

Figure S3. Low-angle XRD patterns for: **(a)** Pt/SBA–BEA,.**(b)** Pd/SBA–BEA and **(c)** Pt-Pd/SBA–BEA catalysts.

It is also crucial to confirm the structure of zeolite in AlSBA-15–zeolite supported catalysts since the synthesis of biporous support relies on AlSBA-15 phase crystallisation in the presence of zeolite particles and in consequence the contact of zeolite particles with the acidic environment takes place. The wide-range XRD diffractograms of Pt-, Pd- and Pt-Pd/SBA–BEA samples (as the examples) (**Figure S4**) show reflexions at *ca.* 12–14° and 22.5° that according to JCPDS 48-0074 are characteristic for BEA [31]. The XRD spectra do not reveal any indication of either long range amorphisation of BEA zeolite or extra framework crystalline compounds. However, the intensity of diffraction signals typical for the zeolite in the composite catalysts is lower compared to pure BEA due to the presence of only 20 *wt%* of zeolite in the biporous catalysts. It is worth noticing that the wide-angle XRD patterns show no diffraction peaks attributed to Pt or Pd. The apparent absence of metal reflections can be caused by too low to be detectable metal loading (0.5 *wt%*). It can also indicate the existence of highly dispersed, small metal crystallites (typically ≤ 2 nm) which are not detectable by XRD. The CO chemisorption measurements do not confirm so high metal dispersion in all catalysts suggesting that the part of the metal must be either partially blocked by some residues originating from the metal precursor, or a considerable part of metal is placed in the support matrix, as being inaccessible species to chemisorption.

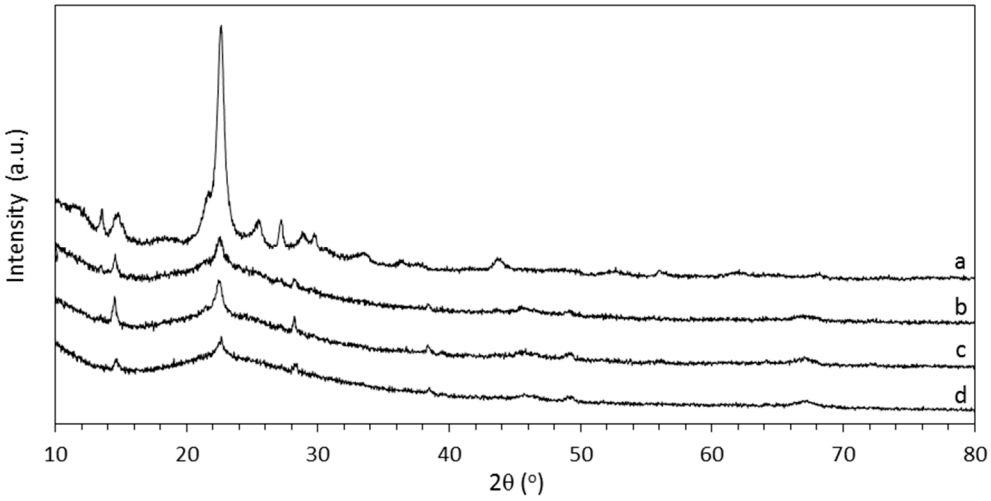

Figure S4. XRD patterns collected for: **(a)** beta zeolite, **(b)** Pt/SBA–BEA, **(c)** Pd/SBA–BEA and **(d)** Pt-Pd/SBA–BEA samples.

1.2. Activity of Pt/zeolite catalysts

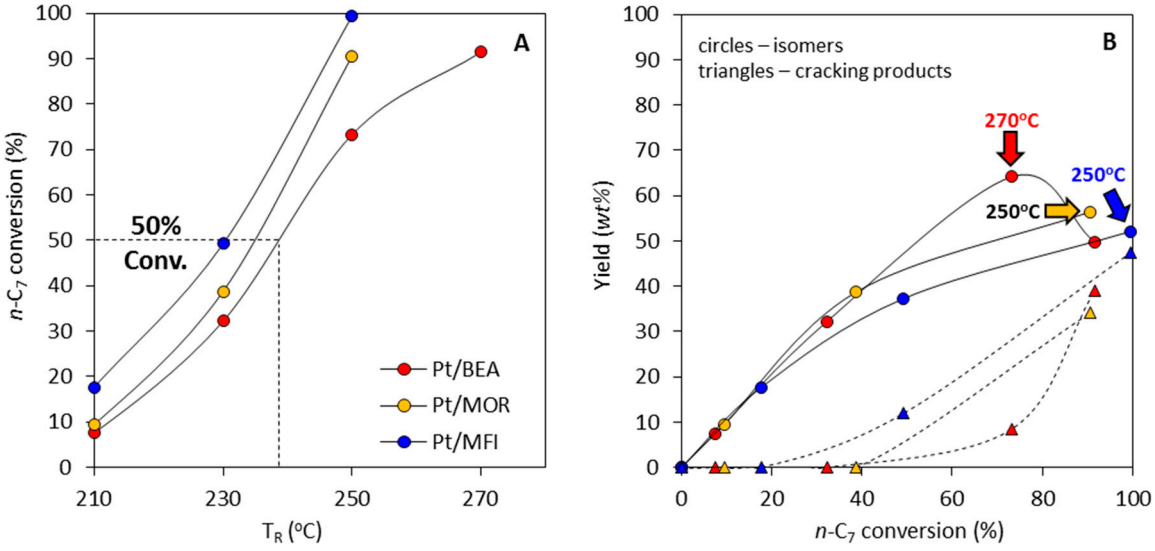

Figure S5. Catalytic performance of the Pt/zeolite catalysts: (**A**) *n*-C7 conversion profiles against TR and (**B**) yield of isomers and cracking products against *n*-C7 conversion for the corresponding catalysts.

1.3. Arrhenius plots

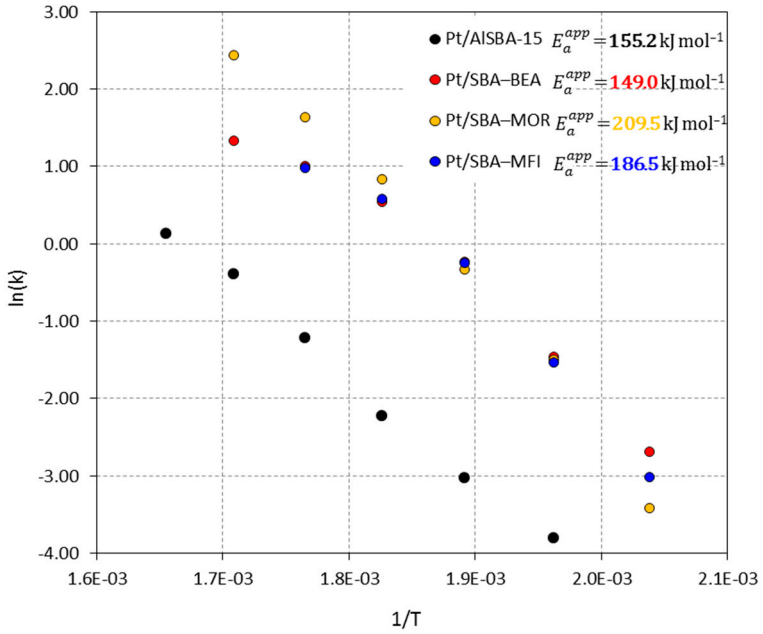

Figure S6. Arrhenius plots *n*-C7 hydroconversion over Pt/AlSBA-15–zeolite catalysts.

1.4. Activity of the catalysts

Table S2. Performance of the catalysts in the hydroconversion of *n*-C7.

Catalyst	T_R (°C)	Conv. (%)	Hydroisomerization				Hydrocracking		Dehydrocyclization	
			total iso-C7 (wt%)	MoBC7[a] (wt%)	MuBC7[b] (wt%)	S_{HISO}[c] (%)	C3+C4 (wt%)	S_{HC}[d] (%)	Aro&CyC (wt%)	$S_{Aro\&CyC}$[e] (%)
Pt/AlSBA-15	250	2.2	2.2	2.2	–	100	–	–	–	–
	270	4.7	4.7	4.7	–	100	–	–	–	–
	290	9.7	8.6	8.6	–	89.4	–	–	1.7	10.6
	310	25.6	21.0	21.0	–	81.8	–	–	4.7	18.2
	330	49.2	42.1	40.4	1.7	85.6	–	—	7.0	14.4
	350	64.5	50.2	44.0	6.1	77.7	6.7	10.4	7.7	11.9
	370	79.3	42.6	34.5	8.1	53.7	18.2	23.0	18.6	23.3
Pt/BEA	230	7.5	7.5	7.5	–	100	–	–	–	–
	250	27.4	27.4	27.4	–	100	–	–	–	–
	270	72.0	63.9	49.2	14.7	88.8	8.1	11.2	–	–
	290	90.7	50.6	34.4	16.2	55.8	37.7	41.6	–	–
	310	94.7	35.5	22.3	13.2	37.4	59.3	62.6	–	–
Pt/MOR	210	9.4	9.4	9.4	–	100	–	–	–	–
	230	38.8	38.8	31.4	7.4	100	–	–	–	–
	250	90.6	56.4	30.1	26.4	62.3	34.2	37.7	–	–
Pt/MFI	210	17.6	17.6	17.6	–	100	–	–	–	–
	230	49.2	37.3	36.2	1.1	75.7	11.9	24.3	–	–
	250	99.5	52.1	27.6	24.5	52.4	47.4	47.6	–	–

[a] MoBC7, *mono*-branched heptane isomers: 2-methylhexane, 3-methylhexane and 3-ethylpentane; [b] MuBC7, *multi*-branched heptane isomers: 2,2-dimethylpentane, 2,3-dimethylpentane, 2,4-dimethylpentane, 3,3-dimethylpentane and 2,2,3-trimethylbutane; [c] S_{HISOM}, selectivity to hydroisomerization products; [d] S_{HC} selectivity to hydrocracking products; [e] $S_{Aro\&CyC}$, selectivity to dehydrocyclization products.

Table S2 (*continued*). Performance of the catalysts in the hydroconversion of *n*-C_7.

Catalyst	T_R (°C)	Conv. (%)	Hydroisomerization				Hydrocracking		Dehydrocyclization	
			total iso-C_7 (wt%)	$MoBC_7$ [a] (wt%)	$MuBC_7$ [b] (wt%)	S_{HISO} [c] (%)	$C_3 + C_4$ (wt%)	S_{HC} [d] (%)	Aro&CyC (wt%)	$S_{Aro\&CyC}$ [e] (%)
Pt/SBA–BEA	230	6.6	6.6	5.7	0.9	100	–	–	–	–
	250	20.7	17.4	17.4	3.0	84.1	–	–	0.1	0.5
	270	54.7	51.4	42.1	9.3	94.0	3.1	5.7	0.2	0.4
	290	82.3	59.7	42.7	16.9	72.5	21.1	25.6	1.5	1.8
	310	93.5	36.9	25.5	11.5	39.5	54.4	58.2	2.1	2.2
	330	97.7	14.1	8.6	5.6	14.4	79.1	81.0	3.6	3.7
Pt/SBA–MOR	230	3.2	3.2	3.2	–	100	–	–	–	–
	250	19.9	19.9	19.9	–	100	–	–	–	–
	270	51.0	51.0	45.1	5.9	100	–	–	–	–
	290	90.1	48.2	30.1	18.1	53.5	41.9	46.5	–	–
	310	99.4	1.0	1.0	–	1.01	96.9	97.48	1.5	1.51
	330	100	–	–	–	–	96.2	96.2	3.8	3.8
Pt/SBA–MFI	230	13.2	11.2	11.2	–	84.8	11.2	84.8	–	–
	250	45.2	37.5	35.8	1.8	83.0	37.5	83.0	–	–
	270	82.0	49.8	45.1	4.7	60.7	49.8	60.7	–	–
	290	96.7	25.0	15.5	9.5	25.9	25.0	25.9	–	–
	310	100	2.5	2.0	0.4	2.50	2.5	2.50	–	–
	330	100	–	–	–	–	–	–	–	–
Pd/SBA–BEA	230	4.1	4.1	4.1	–	100	–	–	–	–
	250	12.1	12.2	9.4	2.8	100	–	–	–	–
	270	32.4	32.4	26.4	6.0	100	–	–	–	–
	290	48.3	38.8	30.6	8.2	80.3	9.5	19.6	0.2	0.1
	310	57.9	29.7	25.3	4.4	51.3	25.9	44.8	2.3	3.9
	330	68.3	17.5	15.6	1.9	25.6	46.2	67.6	4.6	6.8
Pt-Pd/SBA–BEA	230	4.9	4.9	4.9	–	100	–	–	–	–
	250	12.9	12.9	10.4	2.5	100	–	–	–	–
	270	46.5	46.5	39.0	7.5	100	–	–	–	–
	290	78.1	68.2	47.5	20.7	87.4	9.9	12.6	–	–
	310	90.4	59.9	28.5	21.4	66.3	28.1	33.7	–	–
	330	93.5	41.2	19.7	21.5	45.1	52.3	56.0	–	–

[a]$MoBC_7$, *mono*-branched heptane isomers: 2-methylhexane, 3-methylhexane and 3-ethylpentane; [b]$MuBC_7$, *multi*-branched heptane isomers: 2,2-dimethylpentane, 2,3-dimethylpentane, 2,4-dimethylpentane, 3,3-dimethylpentane and 2,2,3-trimethylbutane; [c]S_{HISOM}, selectivity to hydroisomerization products; [d]S_{HC} selectivity to hydrocracking products; [e]$S_{Aro\&CyC}$, selectivity to dehydrocyclization products.

1.5. The catalyst performance in respect to the n-C_7 dehydrocyclization

The product distribution reveal that for Pt/AlSBA-15–zeolite catalysts, isomerization and cracking products account for over 96% of the total reaction products (**Table S2**). Over the composite catalysts the aromatization and cyclization reaction occurs with lower than 4 *wt%* yields. In the investigated temperature range of 230–310°C, *n*-C_7 conversion over the Pt/zeolite catalysts, irrespective of the zeolite type, leads only to isomerization and cracking products. However, the catalytic properties of Pt/AlSBA-15 somewhat differ from those of Pt/AlSBA-15–zeolite and Pt/zeolite. In the case of Pt/AlSBA-15 catalyst the

formation of arenes and cycloalkanes cannot be negligible because, at the reaction temperature range of 330–370°C the yield of aromatization and cyclization products amounts to 7–19 *wt%* (**Table S2**). At the same time, at the temperature range of 330–370°C, it provides the cracking products amounting to 7–18 *wt%* (**Table S2**). It is well known that the scission of C–C bonds and aromatization efficiency increases with increase in the reaction temperature [1]. The catalytic dehydrocyclization of higher alkanes (with at least 6 carbon atoms) occurs *via* two routes: monofunctional (involving metallic sites or acidic sites) and bifunctional mechanism (involving both types of active sites) [2]. Over monofunctional Pt catalysts, involving only the metallic sites, the alkane dehydrocyclization goes mainly *via* two possible pathways. One of these (**Figure S7A**) assumes the dehydrogenation of alkane to yield alkene followed by 1–6 ring closure on the Pt surface involving primary and secondary C–H bond rupture followed by dehydrogenation of the cycloalkanes into aromatics. The 1,5 ring closure (**Figure S7B**) followed by C_5 to C_6 enlargement to a lesser extent also contributes to aromatics production. The third one (**Figure S7C**) consists of the stepwise dehydrogenation of the alkanes into olefins, dienes, and trienes followed by thermal ring closure. According to the monofunctional mechanism (**Figure S7D**), over the acidic sites from the C_6 (or more carbon atoms) alkenes the hydride abstraction at carbon position remote from double bond takes place. The intramolecular attack of the positive charge on the double bond leads to the 1,5 ring closure. Then the transitional C_5 alkylcarbenium ions undergo enlargement giving C_6 carbocations followed by hydrogenation on acid sites. It should be noticed that although the acid-type catalysts appear active in the alkanes aromatization, the produced aromatics yield could not be high since the dominance of the parallel reactions such isomerization and cracking. The described monofunctional pathways cannot be taken into account as predominant in our investigation because the catalysts used by us are bifunctional. In the case of bifunctional catalyst where the metallic sites constitute mostly Pt species and acidic are supplied by the support (the case as in our work), the metallic sites *e.g.* Pt and acidic supplied by the support display an important role in the alkane dehydrocyclization. Accordingly, the dehydrogenation of alkanes into unsaturated intermediates proceeds on the metallic phase, which is followed by terminal 1,6 ring closure of alkene on acidic sites (**Figure S7E**). Next, the dehydrogenation of the cycloalkanes into aromatics takes place over metallic sites. The 1,5 ring closure (**Figure S7F**) followed by C_5 ring enlargement is catalysed by the acid sites of the support but it contributes to a lesser extent in alkanes cyclization. The cracking and isomerization take place as a side reactions, because these acid catalysed steps are usually faster than the dehydrogenation process. In addition, the formation of aromatics with lower number of carbon atoms that the feed (in the case of *n*-heptane transformation, *e.g.* cyclohexane and benzene) may be the result of secondary hydrogenolysis of C_7 aromatics as was found by Jongpatiwut and *co*-workers [3]. This leads to large number of products, the distribution of which is very sensitive to the nature and to the ratio of active sites. Therefore, when the bifunctional catalyst is used, these competing reactions are influenced by the metal particle size, the type and strength of acid sites, the balance between the acid and metal function and also by porous structure of the support. It has been proven that in the presence of bifunctional catalysts, the small Pt particles (high Pt dispersion) favours ring closure, and further dehydrogenation of cyclic intermediates rapidly into aromatics [4]. Also, the moderate acidity of the support is required. Because moderate acidity enables the C_5 enlargement to a C_6 ring and not permits the cracking of the alkene formed by dehydrogenation of the alkane on the metallic sites. Therefore, the bifunctional catalysts showing high acidity and poor metallic function display small activity in the aromatization of alkanes since over these catalysts cracking will prevail with respect to the aromatization. It is also essential to distinguish the role of Brønsted and Lewis acid sites in *n*-C_7 conversion. Being proton-donors Brønsted acid sites play an important role in isomerization and cracking reaction. Tregubenko *et al.* [5] have demonstrated that the activity of Pt/Al_2O_3 catalysts largely depended on the concentration medium-strength Lewis acid sites in high molecular alkanes aromatization.

Let's follow the performance of Pt/AlSBA-15, Pt/BEA and Pt/SBA–BEA composite catalysts in the dehydrocyclization. The comparison of the variations in the dehydrocyclization activity of these catalysts with the variations in the Pt particle size (and Pt dispersion too) and also with the concentration of acid sites has revealed no direct correlation between these quantities. What the results obtained revealed is that the Pt/AlSBA-15 displaying the highest concentration of medium Lewis acid sites together with the lowest strength of Brønsted acid sites provides the highest yield of dehydrocyclization products (up to 19 *wt*%). The results reported on here are consistent with those published by Abudawood *et al.* [6]. They have demonstrated that Lewis acid sites are the mainly contributors to selectivity variations in aromatization of *n*-alkanes over Pt/zeolite catalysts. In the case of Pt/BEA sample, despite the highest dispersion (amounting 75 %) and the smallest Pt particles (which could be an efficient contributors in the aromatization) at the same time the very high concentration and the strength of acid sites makes the catalyst more active in isomerization/cracking reactions.

In spite of the fact that Pt dispersion on the Pt/AlSBA-15 and Pt/SBA–BEA catalysts are quite high and comparable (about 58%), the higher dehydrocyclization efficiency is observed over Pt/AlSBA-15 than over Pt/SBA–BEA one. Over the Pt/SBA–BEA catalyst the yield of aromatization and cyclization products approached only 3.6 *wt*% (**Table S2**). It seems that, the moderate acidity sufficiently balanced by hydrogenation-dehydrogenation function in Pt/SBA–BEA accounts for predomination of isomerization. In other words, the described properties, *i.e.* moderate acidity well balanced by Pt sites in bifunctional catalyst favours rather isomerization than cyclization.

We have also noticed that the most important explanation of differences in the dehydrocyclization properties studied materials lies in the balance between the dehydrogenating function and the Brønsted acid function as well as in the balance between the Lewis and Brønsted acid sites. Thus, in the explanation of differences in dehydrocyclization of the catalysts tested, the effect of the n_{M_A}/n_{PyH^+} as well as n_{PyL}/n_{PyH^+} ratio (where n_{M_A} stands for the number of accessible Pt atoms, n_{PyL} and n_{PyH^+} stands for the number of Lewis and Brønsted acid sites, respectively) are studied (**Table S3**). One can notice that considering the increasing yield of the aromatics and cycloalkanes and the n_{M_A}/n_{PyH^+} ratio the catalysts follow the same order: Pt/BEA < Pt/SBA–BEA < Pt/AlSBA-15. Over the Pt/AlSBA-15 catalyst with the highest n_{M_A}/n_{PyH^+} ratio amounting to 0.26 (**Table S3**) there are large amounts of metal sites near each Brønsted acid sites (displaying also the lowest strength, *i.e.* 0.12) in the metal–acid interfacial region. Because of that, the amount of olefinic intermediates forming on the metal sites is so high that not all are isomerized/cracked over the surrounding Brønsted acid sites but they may partly undertake direct monofunctional 1,6 ring closure over the Pt sites. In the case of Pt/BEA with the lowest n_{M_A}/n_{PyH^+} ratio amounting to 0.08, every metallic site is surrounded by a comparatively high number of Brønsted acid sites, displaying also the highest strength (*i.e.* 0.77). Hence, the lifetime of carbenium ions forming on Brønsted sites is long. In consequence, before carbenium ions are hydrogenated on the Pt sites they may undergo rearrangement and then C–C bond cracking in high extent over the acidic sites.

Whereas, considering the properties of Pt/SBA–BEA catalyst one can noticed that the n_{M_A}/n_{PyH^+} ratio is between these noted for Pt/AlSBA-15 and Pt/BEA and equals 0.17 (**Table S3**). In Pt/SBA–BEA catalyst the sufficient number of Pt sites in the vicinity of Brønsted acid sites (displaying also the moderate strength, *i.e.* 0.16) in the metal–acid interfacial region reduces the average distance between both types of active sites. The shortening the length of diffusion paths facilitates the desorption of branched intermediates and limits other reactions.

A second evaluation that can be made is the comparison between the aromatization efficiency and n_{PyL}/n_{PyH^+} ratio. It reveals that the yield of aromatics&cycloalkanes and n_{PyL}/n_{PyH^+} ratio increases in the same order and that order is found to be: Pt/BEA < Pt/SBA–BEA < Pt/AlSBA-15. Over the Pt/AlSBA-15 catalyst with the highest n_{PyL}/n_{PyH^+}

ratio (it equals 1.56; **Table S3**) there are large amounts of Lewis acid sites near each Brønsted site what may promote the aromatization in some extent. Conversely, the lowest n_{PyL}/n_{PyH^+} ratio in Pt/BEA catalyst (it equals 0.54; **Table S3**) explains the preferential isomerization/cracking. The comparison of the dependence of dehydrocyclization efficiency on the Lewis/Brønsted acid sites ratio in the case of Pt/SBA–BEA has shown that the aromatization occurrence may be reduced by decreasing n_{PyL}/n_{PyH^+} ratio up to 0.69 level (**Table S3**). The reduced n_{PyL}/n_{PyH^+} ratio favours formation of isomers without extensive cracking and aromatization.

To explain the aromatization activity of Pt/AlSBA-15 the porous structure should also be considered. It also worth noting that according to the literature data [4],[7] aromatization occurs over mesoporous catalysts since the presence of mesoporosity facilities hydrogen transfer between olefinic and cyclic intermediates providing the greater yields of aromatics. The presented on here Pt/AlSBA-15 catalyst shows the highest surface of mesopores (**Table S1**) that can contribute in aromatization. Also, the reaction temperature has an effect, since dehydrocyclization of alkanes is an endothermic reaction and therefore thermodynamically favoured at a higher temperature. The Pt/AlSBA-15 catalyst with the lowest acidity is active at considerably higher temperatures as compared to catalyst modified by BEA zeolite what may promote the occurrence of aromatization.

1.6. Reaction pathway for the dehydro-/cyclization of n-alkanes

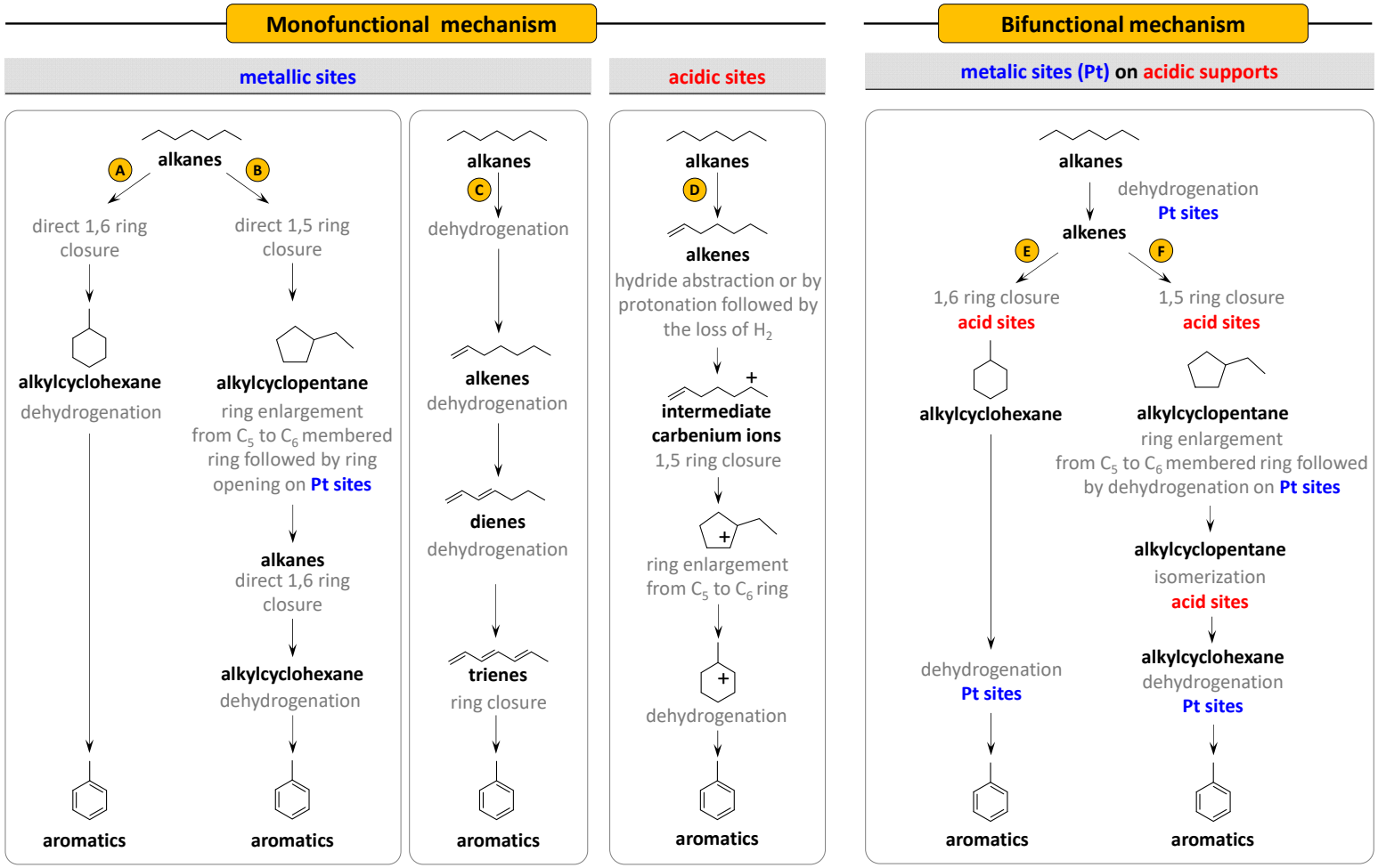

Figure S7. Reaction pathway for the dehydro-/cyclization of n-alkanes over monofunctional and bifunctional catalysts; scheme prepared on the basis of [2].

1.7. Physicochemical characteristics of the catalysts

Table S3. Physicochemical characteristics of the catalysts: ratio of metal to Brønsted acid sites (n_{M_A}/n_{PyH^+}) and Lewis to Brønsted acid sites (n_{PyL}/n_{PyH^+}).

Catalyst	$\frac{n_{M\_A}}{n_{PyH^+}}$	$\frac{n_{PyL}}{n_{PyH^+}}$
Pt/AlSBA-15	0.26	1.56
Pt/BEA	0.08	0.54
Pt/SBA–BEA	0.17	0.69
Pt/SBA–MOR	0.19	1.05
Pt/SBA–MFI	0.09	0.84
Pd/SBA–BEA	0.10	0.69
Pt-Pd/SBA–BEA	0.06	0.77

Note: n_{M_A} number of accessible metal atoms; n_{PyH^+} and n_{PyL} number of Brønsted and Lewis acid sites, respectively.

1.8. Octane number calculation

To judge the catalytic performance for isomerization the research octane number (RON) was calculated according to the following equation [8],[9],[10]:

$$RON = \sum_{i=1}^{k} y_i \, RON_i \quad \text{(S1)}$$

where the RON_i index stands for the pure-component octane number for each molecule (that is labelled as *i*) and y_i is the volume fractions of molecule *i*. The RON numbers were taken from work of Nikolaou et al. [8].

Table S4. Octane number data for hydrocarbons present in isomerization product of *n*-C_7.

Hydrocarbon	RON
2-MeC_6	42.4
3-MeC_6	52
3-EtC_5	65
2,2-DiMeC_5	92.8
2,3-DiMeC_5	92
2,4-DiMeC_5	83.1
3,3-DiMeC_5	80.8
2,2,3-TriMeC_4	112.1

References

1. G. Busca, Chem. Rev. 107 (2007) 5366–5410.
2. P. Mériaudeau, C. Naccache, Catal. Rev. - Sci. Eng. 39 (1997) 5–48.
3. S. Jongpatiwuta, S. Trakarnroek, T. Rirksomboon, S. Osuwan, D.E. Resasco, Catal. Letters 100 (2005) 7–15.
4. N. Parsafard, M.H. Peyrovi, M. Rashidzadeh, Microporous Mesoporous Mater. 200 (2014) 190–198.
5. V.Y. Tregubenko, A.S. Belyi, Kinet. Catal. 61 (2020) 130–136.
6. R.H. Abudawood, F.M. Alotaibi, A.A. Garforth, Ind. Eng. Chem. Res. 50 (2011) 9918–9924.
7. T. Hamoule, M.H. Peyrovi, M. Rashidzadeh, M.R. Toosi, Catal. Commun. 16 (2011) 234–239.
8. N. Parsafard, M. H. Peyrovi, Ni. Parsafard, Reac. Kinet. Mech. Cat. 120 (2017) 231–246.
9. N. Nikolaou, C.E. Papadopoulos, I.A. Gaglias, K.G. Pitarakis, Fuel 83 (2004) 517–523.
10. M. Hasan, A.M. Mohamed, H. Al-Kandari, Mol. Catal. 452 (2018) 1–10.